Materials Research Proceedings 41 (2024) 1009-1016 https://doi.org/10.21741/9781644903131-111

Crystal plasticity-based forming limit analysis for two types of 5052 aluminum alloy sheets with different heat treatment conditions

SATO Sho[1,a *], TSUKAMOTO Maya[1], MAEDA Yasuhiro[2], MAEDA Yasushi[2] and HAMA Takayuki[1,b]

[1]Graduate School of Energy Science, Kyoto University, Kyoto 606-8501, Japan

[2]Technical Development Group, KOBE STEEL, LTD., Kobe 651-2271, Japan

[a] sato.syo.62e@st.kyoto-u.ac.jp, [b]hama@energy.kyoto-u.ac.jp

Keywords: Crystal-Plasticity Analysis, Forming Limit Diagram, Aluminum Alloy, Nakajima Test, Marciniak-Kuczyński Analysis

Abstract. 5000 series aluminum (Al) alloy sheets are increasingly applied to press forming products, such as components used in railroad vehicles and some automobiles, due to their advantages of high specific strength and good corrosion resistance. However, in press forming processes, forming defects, such as failure and wrinkles, often appear. Therefore, it is essential to understand the formability of sheet materials under various stress states and to design appropriate processes to prevent forming-defects occurrence. To evaluate occurrence of failure under various strain states, a Forming Limit Diagram (FLD) is widely used. Although the effects of texture and work-hardening behavior of materials on FLD have been widely studied, their experimental validations are not sufficient. In this study, A5052-O and -H32 Al alloy sheets, which have similar texture and show different work-hardening behavior, are used to investigate the effect of work hardening on the FLD. In the FLDs obtained experimentally, the limit strain under plane-strain tension was larger in the A5052-O sheet with larger work hardening than that of the A5052-H32 sheet with smaller work hardening, whereas that under equibiaxial tension was similar in the two sheets. These trends were reproduced qualitatively well by crystal-plasticity forming limit analyses. The mechanism that yielded these trends were discussed using the simulation results.

Introduction

To facilitate weight reduction of transportation equipment, 5000 series aluminum (Al) alloy sheets are increasingly applied to press forming products, such as components used in railroad vehicles and some automobiles, due to their advantages of high specific strength and good corrosion resistance. However, the ductility of Al alloy sheets is usually not large; thus, the sheets are often suffered from failure during press forming processes. Therefore, it is essential to understand the formability of sheet materials under various stress conditions and to design appropriate forming processes to prevent occurrence of failure.

To evaluate occurrence of failure under various strain conditions, a Forming Limit Diagram (FLD) is widely used [1], in which the safe zone and failure zone is divided by a forming-limit curve (FLC). FLC is obtained by measuring major and minor strains when localized necking occurs under different strain states. FLC is known to be influenced by different factors, including strain rate [2], strain path [3], stress state [4], and temperature [5]. The effects of texture [6] and work hardening [7] of materials have also been widely discussed. However, these studies were usually concerned with virtual materials; thus, experimental validations of numerical results are not sufficient.

In this study, the effects of work hardening on FLCs are investigated experimentally using two types of 5000 series Al alloy sheets with different heat treatment conditions: A5052-O and A5052-H32 sheets. The two sheets have similar texture, whereas they exhibit different work-hardening

behavior. Moreover, crystal-plasticity Marciniak-Kuczyński (MK) analyses are also conducted considering the two Al sheets to investigate the deformation mechanism in detail.

Methods of experiment and simulation

Experimental methods. In this study, the A5052-O and A5052-H32 Al alloy sheets with a thickness of 1.0 mm were used. Hereinafter, these sheets are respectively termed as the O and H32 sheets. The stress-strain curves under uniaxial tension in the rolling direction and pole figures of the two sheets are respectively shown in Figs.1 and 2. Both sheets show similar cube texture. By contrast, they exhibit distinctly different work-hardening behaviors: the yield stress was larger in the H32 sheet than in the O sheet, whereas the work hardening was larger in the O sheet than in the H32 sheet with the work-hardening exponents of 0.239 and 0.157, respectively.

The Nakajima tests [8] were conducted to evaluate FLCs of these sheets. The schematic diagrams of experimental setup and specimen geometry are shown in Fig.3. The test conditions were as follows: after a sheet specimen was clamped between the upper and lower dies, the sheet was stretched using a hemispherical punch with a punch speed of approximately 1 mm/s until failure. To vary the strain ratio, several dumbbell-shape specimens with different width *W* shown in Fig.3(b) were used. To reduce friction between the punch and specimen, a lubrication layer consisting of Vaseline grease, Teflon sheets and PVC sheets was used. A white-black random pattern applied to the specimen surface was captured by CCD cameras, and strains were measured using the Digital Image Correlation (DIC) method (ARAMIS, GOM Corporation). The initiation point of local necking was determined using the "time-dependent" method [9], which identifies the moment when the thickness-strain rate significantly changes at the location where local

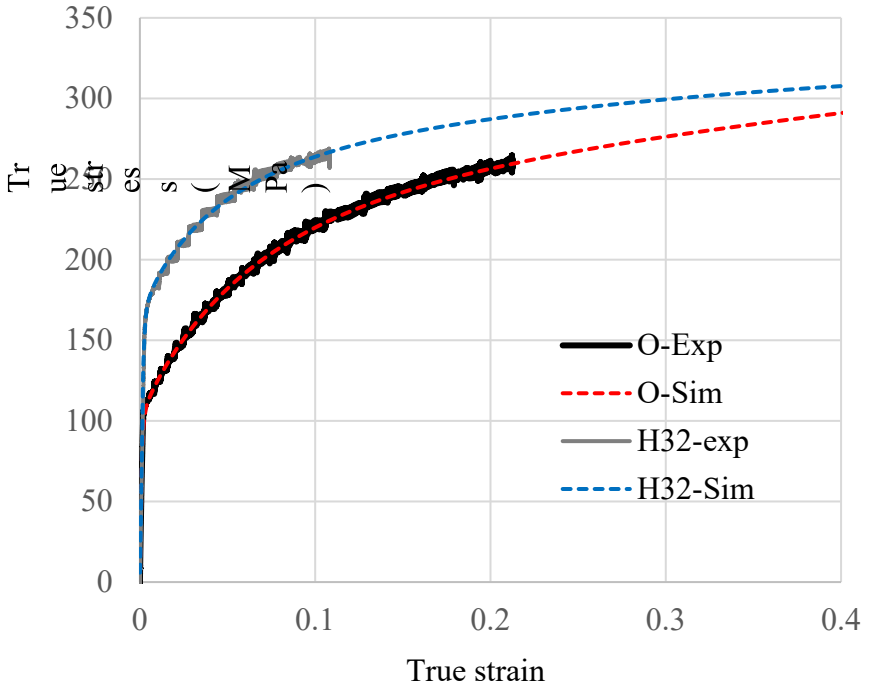

Fig.1 True stress-true strain curves under uniaxial tension of O and H32 sheets.

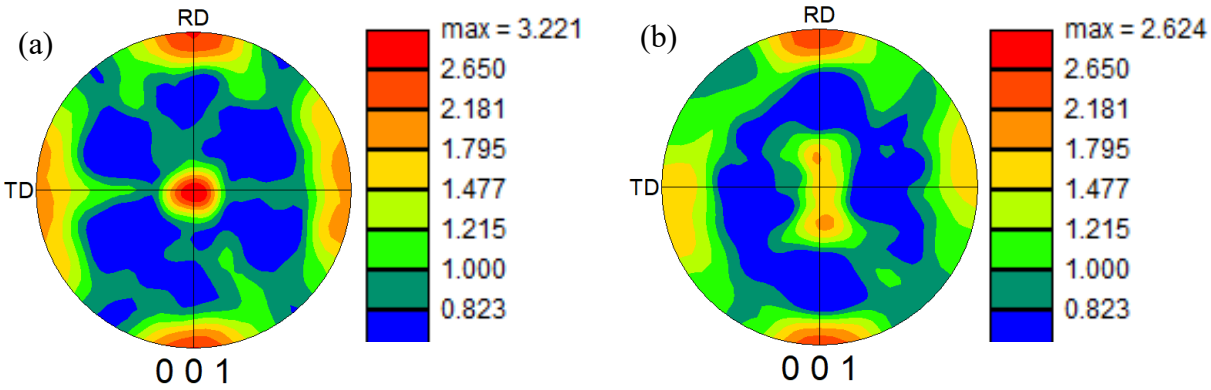

Fig.2 Pole figures of (a)O and (b)H32 sheets.

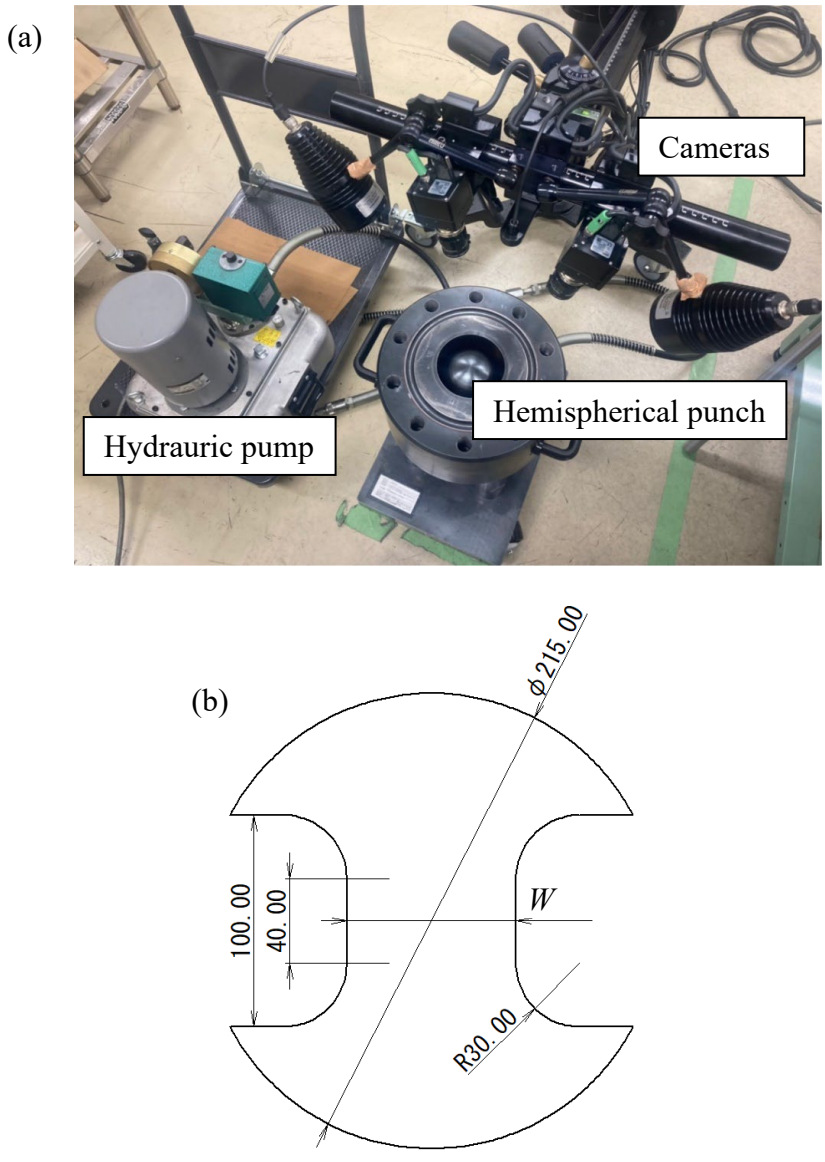

Fig.3 Schematic diagrams of (a)experimental setup and (b)specimen geometry in mm.

Materials Research Proceedings 41 (2024) 1009-1016 https://doi.org/10.21741/9781644903131-111

necking occurs. The tests were performed at least three times for each condition to assure the reproducibility.

Method of simulation. The MK model [10] coupled with an elastic-viscoplastic crystal-plasticity constitutive model was used to evaluate the onset of necking. In the crystal-plasticity model [11,12], the slip rate $\dot{\gamma}^{(\alpha)}$ of slip system α is defined by the following rate-dependent equation:

$$\dot{\gamma}^{(\alpha)} = \dot{\gamma}_0 \left| \frac{\tau^{(\alpha)}}{\tau_Y^{(\alpha)}} \right|^{\frac{1}{m}} \mathrm{sgn}\left(\tau^{(\alpha)}\right) \tag{1}$$

where $\tau_Y^{(\alpha)}$ is the current resistance of the αth slip system. $\dot{\gamma}_0$ is the reference slip rate, and m is the strain rate sensitivity exponent. The rate of slip resistance is given by

$$\dot{\tau}_{\mathrm{Y}}^{(\alpha)} = \sum_{\beta} h_{\alpha\beta} \left| \dot{\gamma}^{(\beta)} \right| \tag{2}$$

where $h_{\alpha\beta}$ is the hardening moduli matrix expressing the interaction of slip systems.

The following dislocation-density-based hardening model was utilized:

$$h_{\alpha\beta} = \frac{\mu}{2} g_{\alpha\beta} \left(\sum_{\kappa} g_{\alpha\kappa} \rho^{(\kappa)} \right)^{-\frac{1}{2}} \left[\frac{1}{K} \left(\sum_{\kappa} g_{\alpha\kappa} \rho^{(\kappa)} \right)^{\frac{1}{2}} - 2 y_c \rho^{(\beta)} \right] \tag{3}$$

where μ is the shear modulus, y_c is characteristic length that represents the annihilation process of dislocation dipoles, K is a material parameter, and $g_{\alpha\beta}$ is the interaction matrix. $\rho^{(\alpha)}$ is the total dislocation density of the αth slip system and its evolution is given by

$$\dot{\rho}^{(\alpha)} = \frac{1}{b} \left(\frac{1}{L^{(\alpha)}} - 2 y_c \rho^{(\alpha)} \right) \left| \dot{\gamma}^{(\alpha)} \right| \tag{4}$$

with b being the magnitude of the Burgers vector. $L^{(\alpha)}$ represents the mean free path and is expressed as $L^{(\alpha)} = K / \sqrt{\sum_{\kappa} g_{\alpha\kappa} \rho^{(\kappa)}}$.

In the analysis, 5000 crystal orientations were considered, and a polycrystalline constitutive equation was derived based on the Taylor assumption [13]. The material parameters were determined to fit the stress-strain curves under uniaxial tension in the rolling direction within uniform elongation ranges, as shown in Fig. 1. An initial imperfection *f*, which is a parameter of the MK model, was determined to match a limit strain under plane-strain tension obtained in experiments. Specifically, *f* was set to 0.9978 and 0.9989 respectively for the O and H32 sheets. The MK analyses were conducted assuming linear strain paths. Although detailed results are presented, the simulation results remained almost unchanged when simulations were conducted under nonlinear strain paths that approximated the experiments.

Results

The experimental and simulation results of FLD are shown in Fig. 4. The horizontal and vertical axes show respectively the minor and major limit strains. In the experimental results, the two sheets exhibited similar V-shaped transitions: the limit strains tended to increase with the increase in the absolute minor strain with a minimum presenting in the first quadrant. By contrast, the transition slopes differed depending on the sheets. The two sheets exhibited similar slopes in the second quadrant, whereas the H32 sheet clearly exhibited a larger slope in the first quadrant than the O sheet. To evaluate the differences in the variation trends between the two materials in more detail, the major limit strain ratio $\varepsilon^*/\varepsilon^*{}_{\rho=0}$ were calculated to normalize the FLDs, where $\varepsilon^*$is the major limit strain and $\varepsilon^*{}_{\rho=0}$ is the major limit strain under plane-strain tension. Fig.5 shows the normalized FLDs. It should be noted that the strain ratio ρ, which is the ratio of the major strain to the minor strain, is used for the horizontal axis to represent clearly the relationship between the biaxial tension states and the limit strain ratios. The two sheets did not show clear differences in

the second quadrant, whereas, in the first quadrant, the limit strain ratios are larger in the H32 sheet than in the O sheet.

The simulation results reproduced qualitatively well the V-shaped transitions and the trend that the limit strain ratios in the first quadrant were larger in the H32 sheet that had smaller work hardening than in the O sheet that had larger work hardening. This result is consistent with a previous study [7]. However, the differences between the two materials observed in the first quadrant were much less pronounced than those of the experimental results.

Discussion

It was reported that the major limit strain ratios in the first quadrant decrease as the yield surface becomes sharper [14-16]. Fig. 6 shows the normalized contours and stress plots of equal plastic work measured at the plastic work of 6.0 MJ/m^3. The stress plots under equibiaxial tension were measured experimentally using an equibiaxial tension test using a cruciform specimen [17]. The contours were determined using the Yld2000-2d function with the exponent M = 8.0 [18]. Although there are only three stress plots on each contour, the contour near equibiaxial tension tended to be sharper in the H32 sheet than in the O sheet in the experiments, whereas the results were almost independent of the material in the simulations, showing that no clear correlation is observed between the FLDs and the contours obtained in this study.

Because of the large difference in the work hardening between the O and H32 sheets, it is hypothesized that the difference in work-hardening behavior between the two sheets is a possible factor that yielded the difference in the FLDs in the first quadrant. To support this hypothesis, the following numerical experiments were conducted. We prepared a virtual O sheet that had the texture of the O sheet and the work-hardening properties of the H32 sheet. It is expected that the virtual O sheet gives higher limit strain ratios in the first quadrant than the original O sheet. f for the virtual O sheet was set to the same value as that for the H32 sheet.

The results are shown in Fig. 7. The original and virtual O sheets exhibited similar limit strain ratios in the second quadrant, whereas the virtual O sheet showed larger limit strain ratios in the first quadrant than the original O sheet, confirming the aforementioned hypothesis. These results show that, even with the same texture, the work-hardening behavior of the H32 sheet leads to larger limit strain ratios in the first quadrant compared to that of the O sheet, indicating that the difference in the work-hardening behavior played an important role in the difference in the first quadrant of the FLC between the O and H32 sheets.

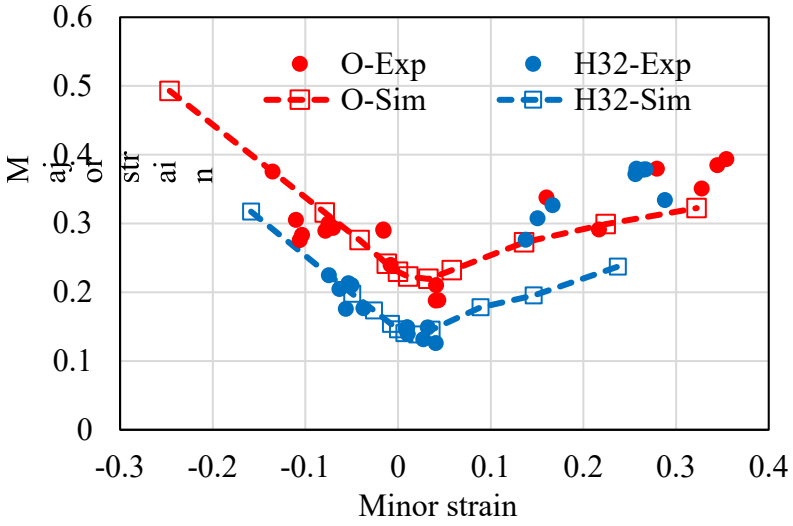

Fig. 4 Experimental and simulation results of FLDs.

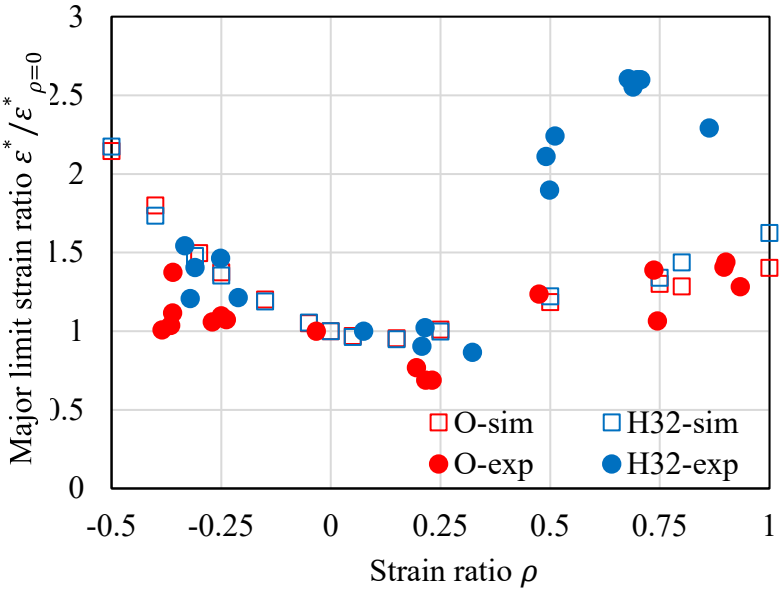

Fig. 5 Normalized FLDs

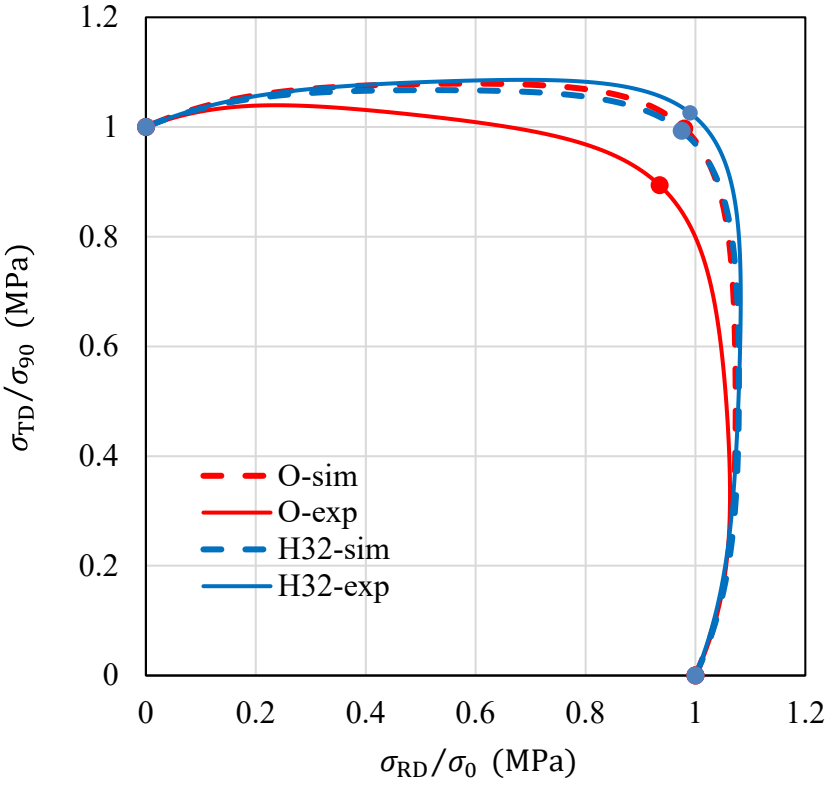

Fig. 6 Normalized contours and stress plots of equal plastic work.

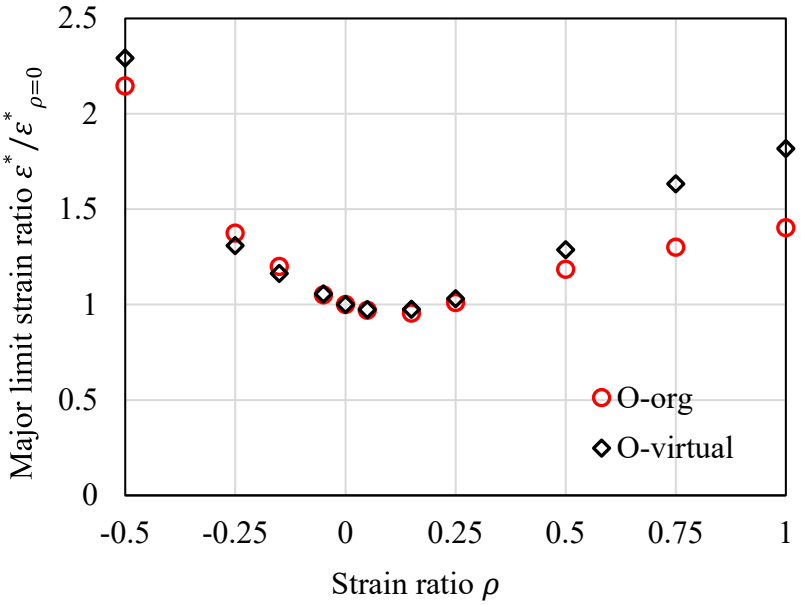

Fig. 7 Simulation results of nomalized FLDs for original and virtual O sheets.

Conclusion

This study evaluated FLCs for A5052-O and A5052-H32 Al alloy sheets which had similar texture and exhibit distinctly different work-hardening behaviors through experiments and numerical analyses. The obtained results are summarized as follows:

1)Experimentally-obtained FLCs showed that the two sheets exhibited similar limit strain ratios in the second quadrant, whereas the H32 sheet clearly exhibited larger limit strain ratios than the O sheet in the first quadrant.

2)Crystal-plasticity MK analyses reproduced qualitatively well the differences in FLCs between the two sheets observed in the experimental results.

3)Numerical experiments showed that the differences in work hardening resulted in the difference in the limit strain ratios in the first quadrant between the two sheets, exhibiting that larger work hardening induces smaller limit strain ratios.

References

[1] S.P. Keeler and W.A. Backofen, Plastic instability and fracture in sheet stretched over rigid punches, ASM Tran. Q. 56 (1963) 25-48.

[2] S.M. Mirfalah-Nasiri, A. Basti and R. Hashemi, Forming limit curves analysis of aluminum alloy considering the through-thickness normal stress, anisotropic yield functions and strain rate, Int. J. Mech. Sci., 117 (2016) 93-101. https://doi.org/10.1016/j.ijmecsci.2016.08.011

[3] A. Werber, W. Nester, M. Grünbaum, K. Wiegand, J. Simon, J. Timm and W. Hotz, Prod. Eng., Assessment of forming limit stress curves as failure criterion for non-proportional forming processes, 7 (2013) 213-221. https://doi.org/10.1007/s11740-013-0446-6

[4] B. Ma, K. Diao, X. Wu, X. Li, M. Wan and Z. Cai, The effect of the through-thickness normal stress on sheet formability, J. Manuf. Process., 21 (2016) 134-140. https://doi.org/10.1016/j.jmapro.2015.12.006

[5] B.L. Ma, M. Wan, X.J. Li, X.D. Wu and S.K. Diao, Evaluation of limit strain and temperature history in hot stamping of advanced high strength steels (AHSS), Int. J. Mech. Sci., 128-129 (2017) 607-613. https://doi.org/10.1016/j.ijmecsci.2017.05.026

[6] K. Yoshida, T. Ishizaki, M. Kuroda and S. Ikawa, The effects of texture on formability of aluminum alloy sheet, Acta. Mater. 55 (2007) 4499-4506. https://doi.org/10.1016/j.actamat.2007.04.014

[7] M. Mohammadi, A. P. Brahme, R. K. Mishra and K. Inal, Effect of post-necking behavior and equivalent stress-strain curves on the accuracy of M-K based forming limit diagrams, Compt. Mater. Sci., 85 (2014) 316-323. https://doi.org/10.1016/j.commatsci.2014.01.017

[8] ISO12004-2:2021 Metallic materials -determination of forming-limit curves for sheet and strip- Part 2: Determination of forming-limit curves in the laboratory.

[9] W. Hotz, M. Merklein, A. Kuppert, H. Friebe and M. Klein, Time dependent FLC determination – Comparison of different algorithms to detect the onset of unstable necking before fracture, Key Eng. Mater., 549 (2013) 397-404. https://doi.org/10.4028/www.scientific.net/KEM.549.397

[10] Z. Marciniak and K. Kuczyński, Limit strains in the processes of stretch-forming sheet metal, Int. J. Mech. Sci., 9 (1967) 609-620. https://doi.org/10.1016/0020-7403(67)90066-5

[11] T. Hama, S. Yagi, K. Tatsukawa, Y. Maeda, Y. Maeda, and H. Takuda, Evolution of plastic deformation behavior upon strain-path changes in an A6022-T4 Al alloy sheet, Int. J. Plast., 137 (2021) 102913. https://doi.org/10.1016/j.ijplas.2020.102913

[12] T. Hama, R. Namakawa, Y. Maeda, and Y. Maeda, Prediction of work-hardening behavior under various loading paths in 5083-O aluminum alloy sheet using crystal plasticity models, Mater. Trans., 62-8 (2021) 1124-1132. https://doi.org/10.2320/matertrans.MT-M2021020

[13] G. I. Taylor, Plastic strain in metals, J. Inst. Metals 62 (1938) 307-324.

[14] F. Barlat, Crystallographic texture, anisotropic yield surfaces and forming limits of sheet metals, Mater. Sci. Eng. 91 (1987) 55-72. https://doi.org/10.1016/0025-5416(87)90283-7

[15] K.W. Neale and E. Chater, Limit strain predictions for strain-rate sensitive anisotropic sheets, Int. J. Mech. Sci. 22 (1980) 563-574. https://doi.org/10.1016/0020-7403(80)90018-1

[16] P.D. Wu, S.R. MacEwen, D.J. Lloyd and K.W. Neale, Effect of cube texture on sheet metal formability, Mater. Sci. Eng. A 364 (2004), 182-187. https://doi.org/10.1016/j.msea.2003.08.020

[17] ISO 16842:2021 Metallic materials – Sheet and strip – Biaxial tensile testing method using cruciform test piece

[18] F. Barlat, J.C. Brem, J.W. Yoon, K. Chung, R.E. Dick, D.J. Lege, F. Pourboghrat, S.-H. Choi, and E. Chu, Plane stress yield function for aluminum alloy sheets – part 1: theory, Int. J. Plast. 19 (2003) 1297-1319. https://doi.org/10.1016/S0749-6419(02)00019-0